Communications

Nanoscale Chemical Imaging of the Reduction Behavior of a Single Catalyst Particle**

Emiel de Smit, Ingmar Swart, J. Fredrik Creemer, Chithra Karunakaran, Drew Bertwistle, Henny W. Zandbergen, Frank M. F. de Groot, and *Bert M. Weckhuysen**

When studying catalyst materials by in situ chemical microspectroscopy, a trade-off is found between the spatial resolution and chemical information of the acquired images. Microscopes utilizing ultraviolet, visible, or infrared radiation often obtain valuable chemical information from the sample, even under reaction conditions.[1–3] However, the spatial resolution of these methods is, in principle, diffraction limited to, in the best cases, several hundreds of nanometers. Conversely, scanning probe techniques[4,5] and electron microscopy (EM)[6,7] offer sub-nanometer resolution. Unfortunately, chemical information is difficult to obtain from these methods, especially under realistic reaction conditions. Scanning transmission X-ray microscopy (STXM)[8] is a novel microspectroscopic technique that has, until now, rarely been used to characterize catalyst materials. STXM combines a high spatial resolution, roughly 15 nm, with high chemical speciation potential by X-ray Absorption Spectroscopy (XAS), using focused soft X-ray light (200–2000 eV) as a probe. The use of the method for characterization of catalyst

materials under realistic conditions was envisioned by Drake et al.,[9] and recently fully exploited by our group.[10] Our STXM nanoreactor system, originally designed for in situ TEM studies,[7] allows treatment of catalytic solids at 1 bar and up to 500°C, while imaging the morphology and the chemical identity of the active phases during reaction. Herein, we report on the reduction behavior of Fe-based Fischer–Tropsch Synthesis (FTS) catalyst by imaging an individual catalyst particle at a resolution of 35 nm using STXM. A separate reduction experiment on the bulk catalyst was carried out to compare reduction phenomena at the nano (local) and macro (global) scale. The extent and rate of reduction of the iron oxide phase on the nanoscale is shown to strongly depend on the extent of interaction with the underlying support oxide.

Iron-based FTS catalysts convert syngas (CO and H_2) into long-chain hydrocarbons by a surface polymerization reaction,[11,12] enabling the production of virtually contaminant (e.g. sulfur)-free chemical feedstocks, such as olefins, and transportation fuels, such as diesel, from sources other than crude oil, such as natural gas, coal, or biomass. Catalyst precursors typically consist of supported or unsupported iron oxide (α-Fe_2O_3 or Fe_3O_4) and it has been shown that the reduction pretreatment of this oxidic phase to a carbidic or metallic (Fe^0) phase is crucial in determining the final FTS performance.[13,14]

The FTS catalyst under study has a starting composition of α-Fe_2O_3, K_2O, CuO, and SiO_2 in relative molar ratios of Fe/Cu/K/Si = 100:7.5:5.9:15.6. K_2O is added to enhance the catalyst performance, whereas CuO is added to improve the reduction rate of the Fe oxide phase. SiO_2 serves as a support material and enhances the dispersion of the iron oxide crystallites. A STXM image of the single catalyst particle under study, before reduction at room temperature, and the average (signal from the whole particle) iron L_3 and L_2 and oxygen K absorption edges, are shown in Figure 1.

The double peak pre-edge feature in the O K edge at around 530 eV[15] and the position of the main L_3 edge peak contribution at 709.3 eV[16] (Figure 1b) indicate that the starting Fe species are present as a pure Fe^{3+} α-Fe_2O_3 phase. This phase is dispersed over the SiO_2 support, as indicated by the extra characteristic contribution in the O K edge spectrum at around 537 eV.[17] The O K edge was fitted to contributions of α-Fe_2O_3 and SiO_2 reference spectra at every 35×35 nm² pixel (Figure 1a; see the Supporting Information). In this way, a chemical component image was reconstructed in which α-Fe_2O_3 is shown in red and SiO_2 in cyan. The resolution of the measurements is not high enough to resolve individual α-Fe_2O_3 crystallites. However, it is clear

[*] E. de Smit, Dr. I. Swart, Dr. F. M. F. de Groot,
Prof. Dr. B. M. Weckhuysen
Inorganic Chemistry and Catalysis
Debye Institute for Nanomaterials Science, Utrecht University
Sorbonnelaan 16, 3584 CA Utrecht (The Netherlands)
Fax: (+31) 30-251-1027
E-mail: f.m.f.degroot@uu.nl
          b.m.weckhuysen@uu.nl

Dr. J. F. Creemer
DIMES-ECTM, Delft University of Technology
P.O. Box 5053, 2600 GB Delft (The Netherlands)

Prof. Dr. H. W. Zandbergen
Kavli Institute of NanoScience, National Centre for High Resolution
Electron Microscopy, Delft University of Technology
P.O. Box 5053, 2600 GB Delft (The Netherlands)

Dr. C. Karunakaran, D. Bertwistle
Canadian Light Source, Inc., University of Saskatchewan
Saskatoon, SK, S7N 0X4 (Canada)

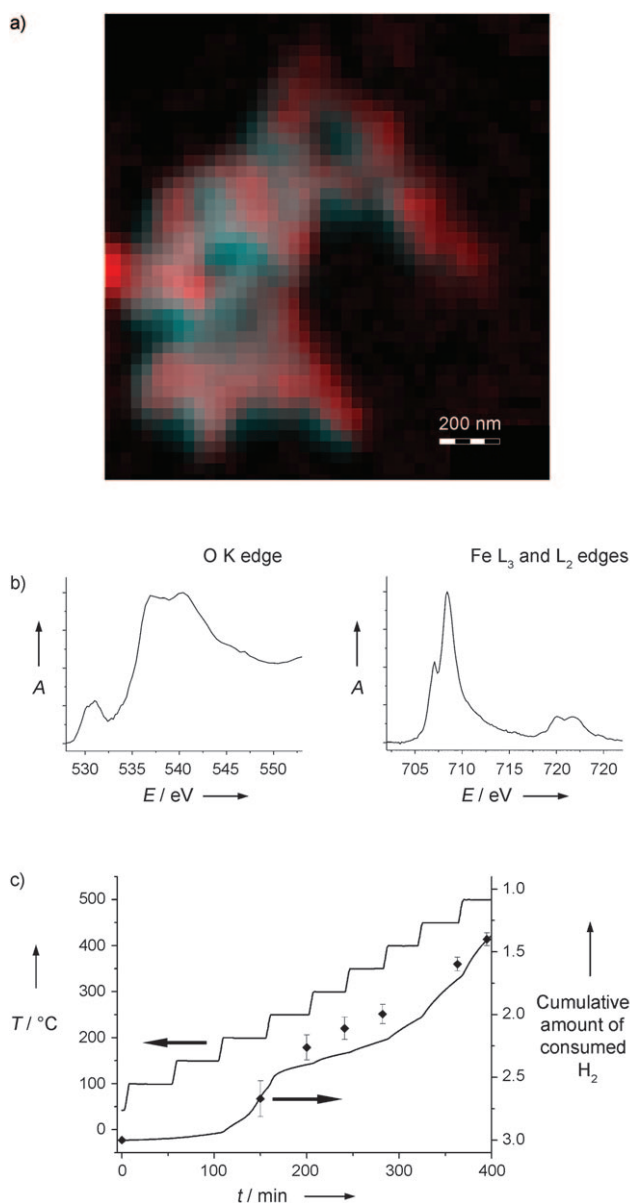Supporting information for this article is available on the WWW under http://dx.doi.org/10.1002/anie.200806003.

Figure 1. a) Chemical component image of the Fe-based FTS catalyst particle before reduction treatment. Red pixels indicate a contribution of the (Fe^{3+}) α-Fe_2O_3 phase, while cyan pixels indicate the presence of SiO_2. The color intensity was normalized to the maximum signal of each species to emphasize the spatial distribution of the species. Pixel dimensions are 35×35 nm^2; b) average O K edge and Fe L_3 and L_2 edges of the catalyst particle before reduction; c) comparison of bulk TPR and STXM reduction data. The temperature program is plotted on the left y axis, the cumulative amount of consumed H_2 on the right y axis. Symbols (♦) indicate the calculated average valence of the catalyst particle as determined by STXM and correspond to the values on the right y axis. Error bars are indicated, assuming 5% error in the fitting procedure.

that the distribution over the SiO_2 support is non-uniform (Figure 1a). The presence of Cu and K in the catalyst was confirmed. However, these species were present in too low concentrations and too high dispersions to image them selectively. Therefore, we focused our study on the Fe and Si phases.

For reference, bulk reduction properties of the material were investigated using temperature programmed reduction (TPR; summarized in Figure 1c). The catalyst was exposed to a flow of H_2 while the temperature was increased, in steps of 50°C, up to 500°C while monitoring the cumulative amount of consumed H_2. Under the assumption of negligible H_2 consumption by reduction of Cu species, this amount can be interpreted as a measure of the extent of reduction of Fe as a function of temperature.

To analyze the influence of local sample morphology on the STXM reduction data, an estimation of the SiO_2 and α-Fe_2O_3 layer thicknesses was made (Figure 2a and the Supporting Information). Three regions of distinct chemical and morphological composition were defined. The first region (region 1) consisted of a thick layer of SiO_2 (ca. 70 nm) and a thick layer of α-Fe_2O_3 (ca. 40 nm), the second region (region 2) of a SiO_2 layer of intermediate thickness (ca. 50 nm) and a thin layer of α-Fe_2O_3 (ca. 20 nm), and finally, a region (region 3) with practically no SiO_2 and a thin layer of α-Fe_2O_3 (ca. 15 nm). Table 1 summarizes the morphological characteristics of these different regions.

The Fe L_3- and L_2-edge X-ray absorption spectra of the three regions at 250°C are shown in Figure 2b. The change in relative abundance of Fe valence in these regions as a function of reduction temperature is shown in Figure 2c (and Figure S1 in the Supporting Information). By performing a least-squares linear combination fitting of the Fe L_3 and L_2 edges at every 35×35 nm^2 pixel, a chemical component image of the catalyst particle was constructed at each reduction temperature (see the Supporting Information). Fe_3O_4, Fe_2SiO_4, and α-Fe were used as references for mixed (1:2) Fe^{2+}/Fe^{3+} (Fe_3O_4), pure Fe^{2+}, and Fe^0 species, respectively. Fe^{3+} has a characteristic main L_3-edge contribution at 709.3 eV, Fe^{2+} at 707.9 eV, and Fe^0 at 706.8 eV (Figure 3, left).[10,16,18] The maximum contribution of the each species was normalized to emphasize the spatial distribution. A valence contour map of the sample (Figure 3, right) was constructed by combining the relative contribution of each species and assigning valence numbers (0 for Fe^0, 2 for Fe^{2+} and $2\frac{2}{3}$ for $Fe^{2+/3+}$) at every pixel.

Up to approximately 200°C, the Fe L_3- and L_2-edge spectra indicated slow reduction of Fe^{3+} in α-Fe_2O_3 to the mixed Fe^{2+} and Fe^{3+} (ratio 1:2) Fe_3O_4 phase. The bulk TPR data (Figure 1c) confirmed that below 200°C hardly any reduction takes place. At 250°C, however, these data show that the material is reduced significantly and differences in reduction behavior were found between the defined regions. It is clear that region 1 largely remains in the mixed Fe^{2+}/Fe^{3+} state (Figure 2b and 3a). The relatively low amount of Fe^{2+} indicates that the material is hardly reduced beyond Fe_3O_4 at this temperature. A significantly higher contribution from Fe^{2+} is observed in region 2. Apparently the SiO_2 phase somehow stabilizes the Fe^{2+} species. This stabilization is usually ascribed to the formation of either FeO or a mixed oxide, such as Fe_2SiO_4.[19,20] In a more elaborate explanation, SiO_2 may interact with the Fe^{2+}/Fe^{3+} Fe_3O_4 spinel phase in such a way that a mixed oxide Fe_2SiO_4 phase is formed.[20] In region 3, the reduction to Fe^0 has made significantly more progress than in the other regions. The thin layer of α-Fe_2O_3 in
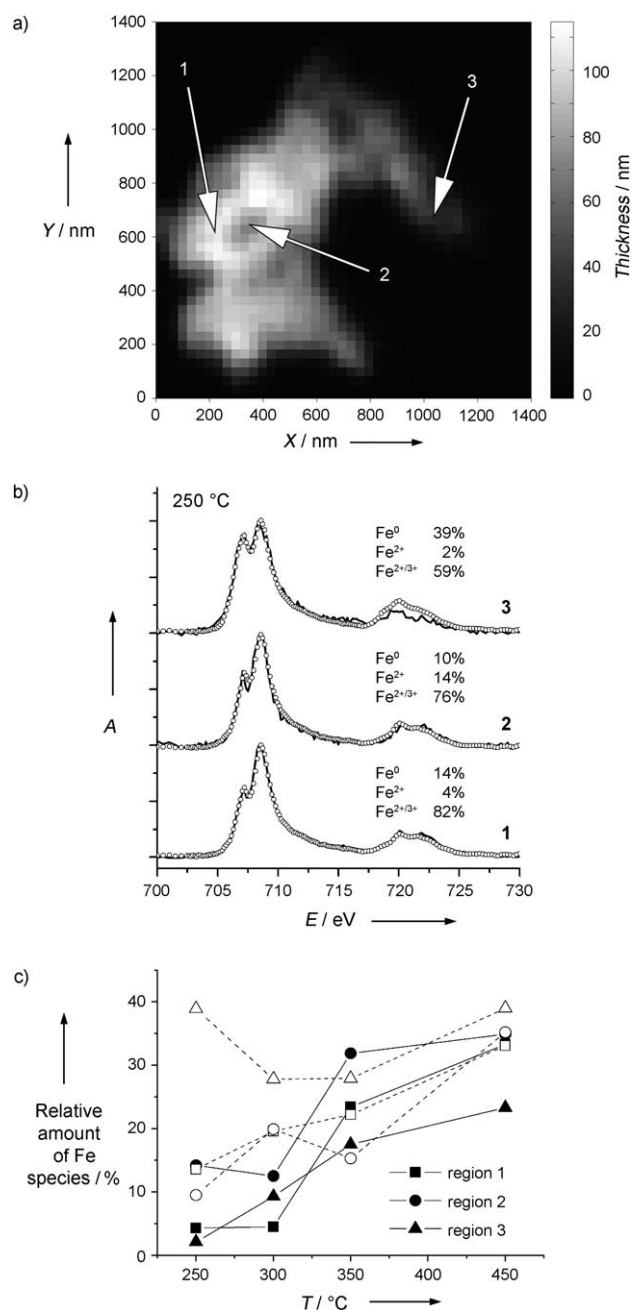
Figure 2. a) Thickness plot of the Fe-based FTS catalyst particle. Pixel dimensions are 35×35 nm^2. b) Fe L$_3$- and L$_2$-edge spectra of the catalyst particle during the reduction treatment at 250°C. Solid lines indicate experimental data from the defined regions in (a). Scattered symbols (○) indicate fitted data. Relative contributions of the different Fe species, resulting from linear combination fitting, are indicated above each spectrum. c) The relative distribution of Fe^0 and Fe^{2+} species as a function of temperature in the different regions. White symbols indicate Fe^0, whereas black symbols indicate Fe^{2+}. The remaining fraction is the amount of Fe$^{2+/3+}$ species.

Table 1: Approximate layer thicknesses (t) for the defined regions under discussion.

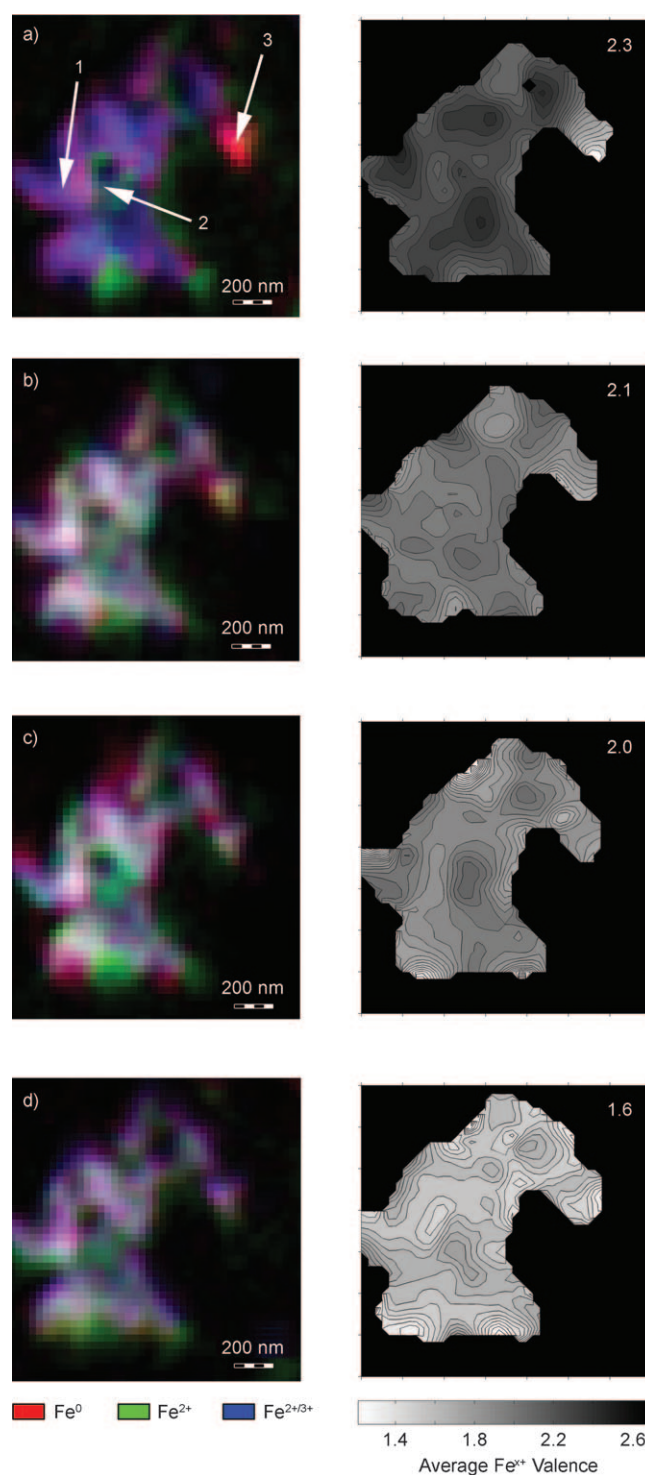| Region	$t_{\alpha\text{-Fe}_2O_3}$ [nm]	t_{SiO_2} [nm]	t_{total} [nm]
1	40	70	110
2	20	50	70
3	15	5	20

Figure 3. Chemical component images of the catalyst particle, showing the spatial distribution of the different iron species (left) and average valence contour maps (right) in 1 bar H$_2$ at a) 250°C, b) 300°C, c) 350°C and d) 450°C. The pixel dimensions (left column) are 35×35 nm^2. The three defined regions are indicated in (a). The average valence of the whole catalyst particle is indicated in the top right corner of the contour maps.

the absence of SiO$_2$ in region 3 apparently leads to fast reduction of Fe^{3+} to Fe^{2+} and Fe^0 species, even at 250°C, as was also measured in additional STXM reduction experi-

ments carried out on bulk α-Fe_2O_3 (Figure S2 in the Supporting Information).

At 300°C, the Fe L edges of region 3 (Figure 2c) show a somewhat lower contribution from Fe^0 and more Fe^{2+} and mixed Fe^{2+}/Fe^{3+} species compared to 250°C. This change might be a direct indication of the migration of $Si(OH)_4$ species over the catalyst.[19–21] Owing to the enhanced mobility of Si species at higher temperatures, induced by reaction with H_2O produced during reduction, SiO_2 may spread over the catalyst, inhibiting the reduction of Fe species beyond Fe^{2+}. In support of this hypothesis, the total thickness of region 3 appeared to increase between 250 and 300°C. An accurate thickness calculation, however, remains difficult owing to the presence of multiple phases. Another explanation for the decrease in relative amount Fe^0 species at 300°C might be a higher mobility for the metallic species. However, this effect is expected to be limited, especially in the case of supported catalysts.[22] Regions 1 and 2 show an enhanced contribution of Fe^{2+} and Fe^0 species and thus a lower average valence (Figure 2c and Figure 3b) compared to 250°C, with the SiO_2-rich region 2 showing a relatively higher abundance of Fe^{2+} species.

Increasing the temperature to 350°C, leads to further reduction for regions 1 and 2 (Figure 2c), with the distribution of Fe species becoming more homogeneous (Figure 3c). However, some regions still show a higher concentration of Fe^0 relative to $Fe^{2+}/(Fe^{2+}/Fe^{3+})$ species and a lower resulting average valence. At 450°C (Figure 3d) all three regions show a $Fe^0/Fe^{2+}/(Fe^{2+}/Fe^{3+})$ species ratio of about 1:1:1. Increasing the temperature to 500°C showed a higher overall contribution of Fe^{2+} and Fe^0 species (Figure S1 in the Supporting Information), but no significant differences in the spatial distribution of Fe species.

In summary, the reduction behavior of a single Fe-based FTS catalyst particle is dependent on its morphology up to 300°C, after which the distribution of Fe over the particle becomes more and more homogeneous with increasing temperature. Fe^{2+} in close contact with SiO_2 is stabilized from further reduction to Fe^0. The mobility of SiO_2 might increase by reaction with H_2O at higher temperatures. As a result, above 300°C, no regions are observed where Fe^0 is the main contributing species. Furthermore, Fe species could not be fully reduced to Fe^0 at temperatures below 500°C. The lowest detected average valence was 1.4 at 500°C, indicating a substantial contribution from Fe^{2+} and Fe^{3+} species. In a more general perspective, we have shown that the use of in situ STXM provides new insights into the local morphologically and chemically dependent reduction behavior of a catalytic solid. It also illustrates the complexity of the interpretation of bulk reduction experiments and their extrapolation to nano-scale phenomena.

Experimental Section

In situ STXM: The experimental setup[10] and nanoreactor[7] are described in detail elsewhere. All experiments were performed on the STXM microscope at beamline 10ID-1 (SM) at the Canadian Light Source in Saskatoon, Canada.[23] Monochromatic X-ray light was focused using a Fresnel-type zone plate lens (outermost zone width 35 nm) resulting in a spatial resolution of about 40 nm. The reactor was mounted on a piezoelectric sample stage, used to focus and produce (x, y) raster scans of the sample. Transmitted light was detected by a scintillator combined with a photomultiplier tube. The nanoreactor consisted of a reactor chamber (ca. $500 \times 500 \times 50$ μm) connected to μm-sized gas channels and equipped with a Pt heater.[7] Owing to the small dimensions involved, the 50°C temperature increments were almost instantaneously achieved. After each increment, the temperature was kept constant for 30 min before acquiring STXM image data.

Temperature programmed reduction (TPR) was performed using a Micromeritics Autochem-II instrument equipped with a TCD detector. Before the experiments, the sample was dried in an Ar flow at 120°C for 20 min. After the TCD signal was stable, the gas stream was switched to 5% H_2/Ar (50 mL min^{-1}). The temperature was raised with increments of 50°C up to 500°C at 20°C min^{-1}. After each increment, the temperature was kept constant for 30 min.

Catalyst: The $Fe_2O_3/CuO/K_2O/SiO_2$ catalyst was synthesized using a reported procedure.[10] The catalyst material was ground, suspended in ethanol, treated in an ultrasonic bath, and loaded by flowing the suspension through the nanoreactor and subsequent drying.

[1] a) M. B. J. Roeffaers, B. F. Sels, H. Uji-i, F. C. De Schryver, P. A. Jacobs, D. E. De Vos, J. Hofkens, *Nature* **2006**, *439*, 572; b) M. B. J. Roeffaers, B. F. Sels, H. Uji-i, B. Blanpain, P. L'Hoest, P. A. Jacobs, F. C. De Schryver, J. Hofkens, D. E. De Vos, *Angew. Chem.* **2007**, *119*, 1736; *Angew. Chem. Int. Ed.* **2007**, *46*, 1706; c) M. B. J. Roeffaers, G. De Cremer, H. Uji-i, B. Muls, B. F. Sels, P. A. Jacobs, F. C. De Schryver, D. E. De Vos, J. Hofkens, *Proc. Natl. Acad. Sci. USA* **2007**, *104*, 12603.

[2] a) M. H. F. Kox, E. Stavitski, B. M. Weckhuysen, *Angew. Chem.* **2007**, *119*, 3726; *Angew. Chem. Int. Ed.* **2007**, *46*, 3652; b) E. Stavitski, M. H. F. Kox, B. M. Weckhuysen, *Chem. Eur. J.* **2007**, *13*, 7057; c) E. Stavitski, M. H. F. Kox, I. Swart, F. M. F. de Groot, B. M. Weckhuysen, *Angew. Chem.* **2008**, *120*, 3599; *Angew. Chem. Int. Ed.* **2008**, *47*, 3543.

[3] a) A. Zürner, J. Kirstein, M. Doblinger, C. Brauchle, T. Bein, *Nature* **2007**, *450*, 705; b) W. Xu, J. S. Kong, Y.-T. E. Yeh, P. Chen, *Nat. Mater.* **2008**, *7*, 992; c) A. Urakawa, N. Maeda, A. Baiker, *Angew. Chem.* **2008**, *120*, 9396; *Angew. Chem. Int. Ed.* **2008**, *47*, 9256.

[4] a) H. H. Rotermund, W. Engel, M. Kordesch, G. Ertl, *Nature* **1990**, *343*, 355; b) T. Zambelli, J. Wintterlin, J. Trost, G. Ertl, *Science* **1996**, *273*, 1688; c) H. Over, Y. D. Kim, A. P. Seitsonen, S. Wendt, E. Lundgren, M. Schmid, P. Varga, A. Morgante, G. Ertl, *Science* **2000**, *287*, 1474; d) S. H. Kim, J. Mendez, J. Wintterlin, G. Ertl, *Phys. Rev. B* **2005**, *72*, 155414.

[5] a) B. L. M. Hendriksen, S. C. Bobaru, J. W. M. Frenken, *Top. Catal.* **2005**, *36*, 43; b) J. W. M. Frenken, B. L. M. Hendriksen, *MRS Bull.* **2007**, *32*, 1015.

[6] a) T. W. Hansen, J. B. Wagner, P. L. Hansen, S. Dahl, H. Topsoe, C. J. H. Jacobsen, *Science* **2001**, *294*, 1508; b) P. L. Hansen, J. B. Wagner, S. Helveg, J. R. Rostrup-Nielsen, B. S. Clausen, H. Topsoe, *Science* **2002**, *295*, 2053; c) P. L. Gai, E. D. Boyes, S. Helveg, P. L. Hansen, S. Giorgio, C. R. Henry, *MRS Bull.* **2007**, *32*, 1044.

[7] J. F. Creemer, S. Helveg, G. H. Hoveling, S. Ullmann, A. M. Molenbroek, P. M. Sarro, H. W. Zandbergen, *Ultramicroscopy* **2008**, *108*, 993.

[8] a) H. Ade in *Experimental Methods in the Physical Sciences*, *Vol. 32* (Eds.: R. Cellota, T. Lucatorto), Academic Press, New York, **1998**, p. 225; b) T. Warwick, K. Franck, J. B. Kortright, G. Meigs, M. Moronne, S. Myneni, E. Rotenberg, S. Seal, W. F. Steele, H. Ade, A. Garcia, S. Cerasari, J. Delinger, S. Hayakawa, A. P. Hitchcock, T. Tyliszczak, J. Kikuma, E. G. Rightor, H. J. Shin, B. P. Tonner, *Rev. Sci. Instrum.* **1998**, *69*, 2964.

[9] I. J. Drake, T. C. N. Liu, M. Gilles, T. Tyliszczak, A. L. D. Kilcoyne, D. K. Shuh, R. A. Mathies, A. T. Bell, *Rev. Sci. Instrum.* **2004**, *75*, 3242.

[10] a) E. de Smit, I. Swart, J. F. Creemer, G. H. Hoveling, M. K. Gilles, T. Tyliszczak, P. J. Kooyman, H. W. Zandbergen, C. Morin, B. M. Weckhuysen, F. M. F. de Groot, *Nature* **2008**, *456*, 222; b) A. T. Bell, *Nature* **2008**, *456*, 185.

[11] M. E. Dry in *Catalysis: Science and Technology, Vol. 1* (Eds.: J. R. Anderson, M. Boudart), Springer, New York, **1981**, p. 160.

[12] E. de Smit, B. M. Weckhuysen, *Chem. Soc. Rev.* **2008**, *37*, 2758.

[13] D. B. Bukur, L. Nowicki, R. K. Manne, X. S. Lang, *J. Catal.* **1995**, *155*, 366.

[14] C. H. Bartholomew, M. W. Stoker, L. Mansker, A. Datye, *Stud. Surf. Sci. Catal.* **1999**, *126*, 265.

[15] F. M. F. de Groot, M. Grioni, J. C. Fuggle, J. Ghijsen, G. A. Sawatzky, H. Petersen, *Phys. Rev. B* **1989**, *40*, 5715.

[16] W. M. Heijboer, A. A. Battiston, A. Knop-Gericke, M. Havecker, R. Mayer, H. Bluhm, R. Schlögl, B. M. Weckhuysen, D. C. Koningsberger, F. M. F. de Groot, *J. Phys. Chem. B* **2003**, *107*, 13069.

[17] T. Sharp, Z. Wu, F. Seifert, B. Poe, M. Doerr, E. Paris, *Phys. Chem. Miner.* **1996**, *23*, 17.

[18] F. M. F. de Groot, A. Kotani, *Core Level Spectroscopy of Solids*, Taylor & Francis, New York, **2008**.

[19] A. F. H. Wielers, A. J. H. M. Kock, C. E. C. A. Hop, J. W. Geus, A. M. van Der Kraan, *J. Catal.* **1989**, *117*, 1.

[20] C. R. F. Lund, J. A. Dumesic, *J. Catal.* **1981**, *72*, 21.

[21] D. H. Everett, J. M. Haynes, P. J. McElroy, *Nature* **1970**, *226*, 1033.

[22] Y. Jin, A. K. Datye, *J. Catal.* **2000**, *196*, 8.

[23] K. V. Kaznatcheev, C. Karunakaran, U. D. Lanke, S. G. Urquhart, M. Obst, A. P. Hitchcock, *Nucl. Instrum. Methods Phys. Res. Sect. A* **2007**, *582*, 96.